Cite as: S. Galeotti *et al.*, *Science* 10.1126/science.aab0669 (2016).

Antarctic Ice Sheet variability across the Eocene-Oligocene boundary climate transition

Simone Galeotti,* Robert DeConto, Timothy Naish, Paolo Stocchi, Fabio Florindo, Mark Pagani, Peter Barrett, Steven M. Bohaty, Luca Lanci, David Pollard, Sonia Sandroni, Franco M. Talarico, James C. Zachos

[1]Dipartimento di Scienze Pure e Applicate, Università degli Studi di Urbino "Carlo Bo," 61029 Urbino, Italy. [2]Department of Geosciences, University of Massachusetts, Amherst, MA, USA. [3]Antarctic Research Centre, Victoria University of Wellington, Wellington, New Zealand. [4]GNS Science, P.O. Box 30368, Lower Hutt, New Zealand. [5]NIOZ Royal Netherlands Institute for Sea Research, Department of Coastal Systems, and Utrecht University, 1790 AB Den Burg, Texel, Netherlands. [6]Istituto Nazionale di Geofisica e Vulcanologia, 00143 Rome, Italy. [7]Department of Geology and Geophysics, Yale University, New Haven, CT, USA. [8]Ocean and Earth Science, University of Southampton, National Oceanography Centre, Southampton SO14 3ZH, UK. [9]Earth System Science Center, Pennsylvania State University, State College, PA, USA. [10]Museo Nazionale dell'Antartide, Università degli Studi di Siena, 53100 Siena, Italy. [11]Dipartimento di Scienze Fisiche, della Terra e dell'Ambiente, Università degli Studi di Siena, 53100 Siena, Italy. [12]Earth Sciences Department, University of California, Santa Cruz, CA 95064, USA.

*Corresponding author. E-mail: simone.galeotti@uniurb.it

About 34 million years ago (Ma) Earth's climate cooled and an ice sheet formed on Antarctica as atmospheric CO_2 fell below ~750 ppm. Sedimentary cycles from a drill core in western Ross Sea provide the first direct evidence of orbitally-controlled glacial cycles between 34–31 Ma. Initially, under atmospheric CO_2 levels ≥ 600 ppm, a smaller Antarctic Ice Sheet, (AIS) restricted to the terrestrial continent, was highly responsive to local insolation forcing. A more stable, continental-scale ice sheet calving at the coastline, did not form until ~32.8 Ma coincident with the first time atmospheric CO_2 levels fell below ~600 ppm. Our results provide new insights into the potential of the AIS for threshold behavior, and its sensitivity to atmospheric CO_2 concentrations above present day levels.

Downloaded from on March 11, 2016

The establishment of the Antarctic Ice Sheet (AIS) is associated with an ~+1.5‰ increase in deep-water marine oxygen isotopic ($\delta^{18}O$) values beginning at ~34 Ma and peaking at ~33.6 Ma (*1–3*), with two positive $\delta^{18}O$ steps separated by ~200 kyr. The first positive isotopic step primarily reflects a temperature decrease (*4*), while the second isotopic step has been interpreted as the onset of a prolonged interval of maximum ice extent (Earliest Oligocene Glacial Maximum or EOGM) between 33.6–33.2 Ma (*5*). Deep-water temperature cooled by 3-5°C (*6*) as a consequence of decreasing CO_2 levels (*7*), while the volume of ice on Antarctica expanded to either near modern dimensions (*6*, *8*) or as much as 25% larger than present day (*9*, *10*). A ~70 m sea-level fall is estimated from low-latitude shallow marine sequences (*9*, *11*). Uncertainties in the magnitudes of these estimates in part reflect the limitations of geochemical proxy records used to deconvolve the relative contribution of ice volume and temperature at orbital resolution (*12*), as well as uncertainties inherent to the backstripping of continental margin sedimentary records (*8*). Ice sheet proximal marine geological records from the continental margin of Antarctica can improve our understanding of the AIS evolution by providing evidence of the direct response of shallow-marine sedimentary environments (e.g., water depth changes) to ice-sheet expansion and retreat.

The temporal pattern and extent of Late Eocene–Early Oligocene (~34.1 Ma to ~31 Ma) Antarctic glacial advance and retreat is recorded in the well-dated CRP-3 drill core, a shallow-water glaciomarine sedimentary succession deposited in the Victoria Land Basin (Fig. 1), tens of kilometres seaward of the present-day East Antarctic Ice Sheet (EAIS) in the Western Ross Sea (*13*). Thirty-seven fluvial to shallow-marine (deltaic) sedimentary cycles occur in the lower 500 m of the drill core (330–780 m below sea-floor; mbsf) that record the advance and retreat of land-terminating glaciers delivering terrigenous sediment to an open wave-dominated coastline and are associated with <20 m oscillations in relative sea-level (RSL) (*14*). These cycles, characterized as 'Type B' (Fig. 2; see also supplementary materials), do not display evidence of ice contact from glacial overriding. In contrast, eleven glaciomarine sedimentary cycles bounded by glacial surfaces of erosion in the upper 300 m of the drillcore (0–300 mbsf) reflect oscillations of the seaward extent of a marine-terminating ice sheet onto the Ross Sea continental shelf and across the CRP-3 drill site associated with larger RSL fluctuations of >20 m (*14*) (Type A cycles in Fig. 2; see also supplementary materials). Temporal variations in lithofacies, grain-size, and clast abundance primarily reflect oscillations in depositional energy that were controlled by changes in water depth and/or glacial proximity (*14*, *15*). Shallow marine sedimentary cycles analogous to those observed in the CRP-3 drillcore have been directly linked with orbitally driven climatic cycles of the AIS across the Oligocene-Miocene boundary at a nearby Ross Sea site (*15*). Ac-

cordingly, we apply a similar approach to directly compare the timing of proximal ice-volume changes during the Early Oligocene against high-resolution temperature and ice-volume proxy records derived from distal deep-sea sequences.

Clast abundance (Fig. 2) reflects glacial proximity and has been shown in a previous study to be controlled by orbital forcing in conjunction with the deposition of Type B cycles in the lower part of CRP-3 (*16*). To similarly test for the role of orbital forcing within the laterally extensive glacial advances within the Type A cycle succession in the upper 300 m of the CRP-3 core, we apply a Singular Spectrum Analysis (see supplementary materials) to the clast abundance time series and a new record of luminance, which reflects changing proportions of clay and sand in sedimentary environments controlled by the proximity to the ice margin and by changes in water depth associated with RSL fluctuations (*14*). An independently derived age model for CRP-3, based on biochronologic calibration of a magnetic reversal stratigraphy (*16*), together with identification of the orbital components in these records enables a one-to-one correlation of sedimentary cycles to the highly-resolved, orbitally tuned $\delta^{18}O$ record from the deep sea (*2*, *17*) (Fig. 2). A key age constraint in the CRP-3 record is the precisely dated transition (+/− 5-kyrs) at 31.1 Ma between magnetic polarity Chrons C12n/C12r at 12.5 mbsf (*13*) (fig. S5).

Variation in facies and clast abundance within Type B shallow-marine sedimentary cycles have previously been interpreted to reflect periodic advance and retreat of land terminating alpine glaciers in the Transantarctic Mountains (*15*) in response to precession and obliquity forcing (*16*) (Fig. 2). This direct response to orbitally paced local insolation forcing indicates a highly dynamic AIS that advanced and retreated during the early icehouse phase of the EOGM. The first sedimentary evidence of ice advance onto the Ross Sea continental shelf coincides with the deposition of unconformity bound, Type A sedimentary cycles beginning at 32.8 Ma, and marks an abrupt transition in AIS sensitivity to orbital forcing that was paced by longer-duration eccentricity cycles (Figs. 2 and 3). This phase is also associated with climate cooling and increased physical weathering as evidenced by a change in clay mineralogy (*18*). Type A cycles (Fig. 2) have been interpreted to represent cyclic alternations in both grounding-line proximity and RSL change (*14*). According to Glacial Isostatic Adjustment (GIA) theory and given the ice marginal position of the CRP-3 site, any proximal ice-thickness variation would have triggered crustal and geoidal deformations such that the resulting local RSL change would be opposite in sign to eustatic trends and likely of larger amplitude (see supplementary materials). However, sedimentological evidence implies that glacial maxima and minima locally coincided with times of minimum and maximum RSL, respectively, for both Type A or Type B cycles (*14*). This implies that the GIA-induced RSL rise that was caused by the expansion and grounding of the ice sheet at the CRP-3 site was counter-balanced by a strong RSL drop as a consequence of the forebulge uplift driven by synchronous EAIS thickening. Therefore, we argue that the appearance of marine-grounded ice near the CRP-3 site was enhanced by flexural crustal uplift as the Eastern Antarctic Ice Sheet expanded, resulting in a RSL fall (> 40 m) in phase with the hypothetical eustatic trend.

Both petrological and apatite fission track evidence (*19*) suggests that diamictites deposited as part of 400 kyr sedimentary cycles spanning ~17–157 mbsf (~32.0–31.1 Ma; Fig. 2), were derived both locally from the Mackay glacier and from the southern Transantarctic Mountains outlet glaciers during glacial overriding and downcutting. Flowlines that trend northwestward into McMurdo Sound from the Byrd, Skelton and Mulock glaciers are implied by model simulation of the early Oligocene glacial expansion (*10*, *20*).

Based on our chronology and geological evidence for ice-grounding, a marine calving ice sheet first occurred in western Ross Embayment at ~32.8 Ma, approximately one million years after the glacial maximum (Oi1) inferred by $\delta^{18}O$ values from marine carbonate isotope records (*17*) (Figs. 2 and 3). Oxygen isotope values paired with southern high-latitude Mg/Ca records (*3*) indicate that the AIS volume was slightly larger across Oi1a (~32.8 Ma) than across the EOGM. Importantly, the Oi1a shift coincides – within the degree of uncertainty shown in Fig. 3 (see also fig. S17) – with the CO_2 minimum (~600 ppmv) at the end of a ~40% decline beginning in the late Eocene (*7*, *21*) (Fig. 3). Declining CO_2 levels that culminate during Oi1a are fully consistent with model-derived CO_2 thresholds for Antarctic glaciation (*20*). The Oi1a interval also corresponds to a long-term minimum in eccentricity and obliquity (*22*), similar to the orbital configuration favoring the onset of glaciation across Oi1 (Fig. 3), implying that an extended period of low seasonality with cooler summers contributed to these long period glacial maxima.

Therefore, we argue that in spite of ice expansion during the EOGM, the nascent AIS was strongly sensitive to orbitally paced, local insolation forcing until a CO_2 threshold of ~600 ppmv was crossed at 32.8 Ma (Fig. 3 and fig. S17). After 32.8Ma, an expanded continental-scale ice sheet displayed progressively stronger orbital ice-sheet hysteresis — behavior that is also suggested by ice models (*20*, *23*). Our observations from the CRP-3 record are also consistent with far-field ice volume proxies that indicate RSL changes of ~25 m in the time interval between 33.4-32.8 Ma (*9*, *11*), equivalent to ~40% of present-day AIS volume. Whereas, after 32.8 Ma, a protracted period of RSL stability is observed in $\delta^{18}O$ records, which corresponds with our proxi-

mal evidence for an AIS that was relatively insensitive to higher frequency orbital forcing (*11*) until ~29 Ma, when CO_2 values again increase to above 600 ppm (*24*) (fig. S17). Our observation of AIS history and behavior lead us to conclude that the partial pressure of atmospheric CO_2 was the primary influence on the overall climate state and variability of AIS volume, including its sensitivity to orbital forcing, which implies a close linkage between carbon cycle dynamics and AIS evolution on both long-period and short-period orbital time scales. Indeed, amplification of the long-period eccentricity component — observed in the CRP-3 record at ~32 Ma — tracks the establishment of low-latitude $\delta^{13}C$ variability with a 405-kyr periodicity (*25*).

The general orbital coherence and phasing between glacial cycles and marine $\delta^{13}C$ records (Fig. 2) indicates that carbon cycle feedbacks contributed to CO_2 changes and amplification of short- and long-period eccentricity-paced glacial-interglacial cycles in the Early Oligocene (*26*), similar to the climate-carbon cycle dynamics associated with Northern Hemisphere glacial cycles during the Pleistocene. Coupled global climate-ice sheet models predict that the AIS should display threshold-like behavior in response to long-term trends in atmospheric CO_2 levels (*20*). For example the stability threshold for marine-based sectors of the AIS has been shown to be ~400ppm, and between 300-400ppm marine ice sheets are highly dynamic in response to orbital forcing (*27*, *28*). Inter-model comparisons suggest a larger range of atmospheric CO_2 values (~ 560–920 ppm) for AIS glaciation (*29*). Data presented in this study imply that a CO_2 threshold for a continental-scale Antarctic ice sheet occurred at ~600 ppm, and AIS sensitivity to insolation forcing and vulnerability to melt increases dramatically between 600-750ppm.

REFERENCES AND NOTES

1. J. C. Zachos, T. M. Quinn, K. A. Salamy, High-resolution (10^4 years) deep-sea foraminiferal stable isotope records of the Eocene-Oligocene climate transition. *Paleoceanography* **11**, 251–266 (1996). doi:10.1029/96PA00571
2. H. K. Coxall, P. A. Wilson, H. Pälike, C. H. Lear, J. Backman, Rapid stepwise onset of Antarctic glaciation and deeper calcite compensation in the Pacific Ocean. *Nature* **433**, 53–57 (2005). Medline doi:10.1038/nature03135
3. S. M. Bohaty, J. C. Zachos, M. L. Delaney, Foraminiferal Mg/Ca evidence for Southern Ocean cooling across the Eocene-Oligocene transition. *Earth Planet. Sci. Lett.* **317–318**, 251–261 (2012). doi:10.1016/j.epsl.2011.11.037
4. C. H. Lear, T. R. Bailey, P. N. Pearson, H. K. Coxall, Y. Rosenthal, Cooling and ice growth across the Eocene-Oligocene transition. *Geology* **36**, 251 (2008). doi:10.1130/G24584A.1
5. Z. Liu, S. Tuo, Q. Zhao, X. Cheng, W. Huang, Deep-water Earliest Oligocene Glacial Maximum (EOGM) in South Atlantic. *Chin. Sci. Bull.* **49**, 2190–2197 (2004). doi:10.1007/BF03185787
6. Z. Liu, M. Pagani, D. Zinniker, R. Deconto, M. Huber, H. Brinkhuis, S. R. Shah, R. M. Leckie, A. Pearson, Global cooling during the eocene-oligocene climate transition. *Science* **323**, 1187–1190 (2009). Medline doi:10.1126/science.1166368
7. M. Pagani, J. C. Zachos, K. H. Freeman, B. Tipple, S. Bohaty, Marked decline in atmospheric carbon dioxide concentrations during the Paleogene. *Science* **309**, 600–603 (2005). Medline doi:10.1126/science.1110063
8. K. G. Miller, J. V. Browning, M.-P. Aubry, B. S. Wade, M. E. Katz, A. A. Kulpecz, J. D. Wright, Eocene-Oligocene global climate and sea-level changes: St. Stephens Quarry, Alabama. *Bull. Geol. Soc. Am.* **120**, 34–53 (2008). doi:10.1130/B26105.1
9. M. E. Katz, K. G. Miller, J. D. Wright, B. S. Wade, J. V. Browning, B. S. Cramer, Y. Rosenthal, Stepwise transition from the Eocene greenhouse to the Oligocene icehouse. *Nat. Geosci.* **1**, 329–334 (2008). doi:10.1038/ngeo179
10. D. S. Wilson, D. Pollard, R. M. DeConto, S. S. R. Jamieson, B. P. Luyendyk, Initiation of the West Antarctic Ice Sheet and estimates of total Antarctic ice volume in the earliest Oligocene. *Geophys. Res. Lett.* **40**, 4305–4309 (2013). doi:10.1002/grl.50797
11. K. G. Miller, M. A. Kominz, J. V. Browning, J. D. Wright, G. S. Mountain, M. E. Katz, P. J. Sugarman, B. S. Cramer, N. Christie-Blick, S. F. Pekar, The Phanerozoic record of global sea-level change. *Science* **310**, 1293–1298 (2005). Medline doi:10.1126/science.1116412
12. K. Billups, D. P. Schrag, Application of benthic foraminiferal Mg/Ca ratios to questions of Cenozoic climate change. *Earth Planet. Sci. Lett.* **209**, 181–195 (2003). doi:10.1016/S0012-821X(03)00067-0
13. F. Florindo, G. S. Wilson, A. P. Roberts, L. Sagnotti, K. L. Verosub, Magnetostratigraphic chronology of a late Eocene to early Miocene glacimarine succession from the Victoria Land Basin, Ross Sea, Antarctica. *Global Planet. Change* **45**, 207–236 (2005). doi:10.1016/j.gloplacha.2004.09.009
14. C. R. Fielding, T. R. Naish, K. J. Woolfe, Facies architecture of the CRP-3 Drillhole, Victoria Land Basin, Antarctica. *Terra Antarctica* **8**, 217–224 (2001).
15. T. R. Naish, K. J. Woolfe, P. J. Barrett, G. S. Wilson, C. Atkins, S. M. Bohaty, C. J. Bücker, M. Claps, F. J. Davey, G. B. Dunbar, A. G. Dunn, C. R. Fielding, F. Florindo, M. J. Hannah, D. M. Harwood, S. A. Henrys, L. A. Krissek, M. Lavelle, J. van Der Meer, W. C. McIntosh, F. Niessen, S. Passchier, R. D. Powell, A. P. Roberts, L. Sagnotti, R. P. Scherer, C. P. Strong, F. Talarico, K. L. Verosub, G. Villa, D. K. Watkins, P. N. Webb, T. Wonik, Orbitally induced oscillations in the East Antarctic ice sheet at the Oligocene/Miocene boundary. *Nature* **413**, 719–723 (2001). Medline doi:10.1038/35099534
16. S. Galeotti, L. Lanci, F. Florindo, T. R. Naish, L. Sagnotti, S. Sandroni, F. M. Talarico, Cyclochronology of the Eocene-Oligocene transition from the Cape Roberts Project-3 core, Victoria Land basin, Antarctica. *Palaeogeogr. Palaeoclimatol. Palaeoecol.* **335–336**, 84–94 (2012). doi:10.1016/j.palaeo.2011.08.011
17. H. K. Coxall, P. A. Wilson, Early Oligocene glaciation and productivity in the eastern equatorial Pacific: Insights into global carbon cycling. *Paleoceanography* **26**, PA2221 (2011). doi:10.1029/2010PA002021
18. W. Ehrmann, M. Setti, L. Marinoni, Clay minerals in Cenozoic sediments off Cape Roberts (McMurdo Sound, Antarctica) reveal palaeoclimatic history. *Palaeogeogr. Palaeoclimatol. Palaeoecol.* **229**, 187–211 (2005). doi:10.1016/j.palaeo.2005.06.022
19. V. Olivetti, M. L. Balestrieri, F. Rossetti, F. M. Talarico, Tectonic and climatic signals from apatite detrital fission track analysis of the Cape Roberts Project core records, South Victoria Land, Antarctica. *Tectonophysics* **594**, 80–90 (2013). doi:10.1016/j.tecto.2013.03.017
20. R. M. DeConto, D. Pollard, Rapid Cenozoic glaciation of Antarctica induced by declining atmospheric CO_2. *Nature* **421**, 245–249 (2003). Medline doi:10.1038/nature01290
21. P. N. Pearson, G. L. Foster, B. S. Wade, Atmospheric carbon dioxide through the Eocene-Oligocene climate transition. *Nature* **461**, 1110–1113 (2009). Medline doi:10.1038/nature08447
22. J. Laskar, P. Robutel, F. Joutel, M. Gastineau, A. C. M. Correia, B. Levrard, A long-term numerical solution for the insolation quantities of the Earth. *Astron. Astrophys.* **428**, 261–285 (2004). doi:10.1051/0004-6361:20041335
23. D. Pollard, R. M. DeConto, Hysteresis in Cenozoic Antarctic ice-sheet variations. *Global Planet. Change* **45**, 9–21 (2005). doi:10.1016/j.gloplacha.2004.09.011
24. Y. G. Zhang, M. Pagani, Z. H. Liu, S. M. Bohaty, R. DeConto, A 40-million-year history of atmospheric CO_2. *Philos. Trans. R. Soc. A* **371**, 20130096 (2013). doi:10.1098/rsta.2013.0096
25. H. Pälike, R. D. Norris, J. O. Herrle, P. A. Wilson, H. K. Coxall, C. H. Lear, N. J. Shackleton, A. K. Tripati, B. S. Wade, The heartbeat of the Oligocene climate system. *Science* **314**, 1894–1898 (2006). doi:10.1126/science.1133822 Medline

26. J. C. Zachos, L. R. Kump, Carbon cycle feedbacks and the initiation of Antarctic glaciation in the earliest Oligocene. *Global Planet. Change* **47**, 51–66 (2005). doi:10.1016/j.gloplacha.2005.01.001
27. M. O. Patterson, R. McKay, T. Naish, C. Escutia, F. J. Jimenez-Espejo, M. E. Raymo, S. R. Meyers, L. Tauxe, H. Brinkhuis, A. Klaus, A. Fehr, J. A. P. Bendle, P. K. Bijl, S. M. Bohaty, S. A. Carr, R. B. Dunbar, J. A. Flores, J. J. Gonzalez, T. G. Hayden, M. Iwai, K. Katsuki, G. S. Kong, M. Nakai, M. P. Olney, S. Passchier, S. F. Pekar, J. Pross, C. R. Riesselman, U. Röhl, T. Sakai, P. K. Shrivastava, C. E. Stickley, S. Sugasaki, S. Tuo, T. van de Flierdt, K. Welsh, T. Williams, M. Yamane, Orbital forcing of the East Antarctic ice sheet during the Pliocene and Early Pleistocene. *Nat. Geosci.* **7**, 841–847 (2014). doi:10.1038/ngeo2273
28. G. L. Foster, E. J. Rohling, Relationship between sea level and climate forcing by CO_2 on geological timescales. *Proc. Natl. Acad. Sci. U.S.A.* **110**, 1209–1214 (2013). Medline doi:10.1073/pnas.1216073110
29. E. Gasson, D. J. Lunt, R. DeConto, A. Goldner, M. Heinemann, M. Huber, A. N. LeGrande, D. Pollard, N. Sagoo, M. Siddall, A. Winguth, Uncertainties in the modelled CO_2 threshold for Antarctic glaciation. *Clim. Past Discuss.* **9**, 5701–5745 (2014). doi:10.5194/cpd-9-5701-2013
30. S. Sandroni, F. Talarico, Petrography and provenance of basement clasts and clast variability in CRP-3 drillcore (Victoria Land Basin, Antarctica). *Terra Antarctica* **8**, 449–467 (2001).
31. Cape Roberts Science Team, Studies from the Cape Roberts Project, Ross Sea, Antarctica. Initial report on CRP-3. *Terra Antarctica* **7**, 1–209 (2000).
32. R. D. Powell, M. G. Laird, T. R. Naish, C. R. Fielding, L. A. Krissek, J. J. M. van der Meer, Depositional environments for strata cored in CRP-3 (Cape Roberts Project), Victoria Land Basin Antarctica: Palaeoglaciological and palaeoclimatological inferences. *Terra Antarctica* **8**, 207–216 (2001).
33. T. R. Naish, P. J. Barrett, G. B. Dunbar, K. J. Woolfe, A. G. Dunn, S. A. Henrys, M. Claps, R. D. Powell, C. R. Fielding, Sedimentary cyclicity in CRP Drillcore, Victoria Land Basin, Antarctica. *Terra Antarctica* **8**, 225–244 (2001).
34. G. B. Dunbar, T. R. Naish, P. J. Barrett, C. R. Fielding, R. D. Powell, Constraining the amplitude of late Oligocene bathymetric changes in Western Ross Sea during orbitally-induced oscillations in the East Antarctic Ice Sheet: (1) Implications for glacimarine sequence stratigraphic models. *Palaeogeogr. Palaeoclimatol. Palaeoecol.* **260**, 50–65 (2008). doi:10.1016/j.palaeo.2007.08.018
35. S. A. Henrys *et al*., *Antarctica: A Keystone in a Changing World-Online Proceedings for the Tenth International Symposium on Antarctic Earth Sciences*, 4 (2007).
36. C. R. Fielding, J. Whittaker, S. A. Henrys, T. J. Wilson, T. R. Naish, Seismic facies and stratigraphy of the Cenozoic succession in McMurdo Sound, Antarctica: Implications for tectonic, climatic and glacial history. *Palaeogeogr. Palaeoclimatol. Palaeoecol.* **260**, 8–29 (2008). doi:10.1016/j.palaeo.2007.08.016
37. P. G. Fitzgerald, E. Stump, Cretaceous and Cenozoic episodic denudation of the Transantarctic Mountains, Antarctica: New constraints from apatite fission track thermochronology in the Scott Glacier region. *J. Geophys. Res.* **102**, 7747–7765 (1997). doi:10.1029/96JB03898
38. P. J. Barrett, Grain-size analysis of samples from Cape Roberts Core CRP-3, Victoria Land Basin, Antarctica, with inferences about depositional setting and environment. *Terra Antarctica* **8**, 245–254 (2001).
39. M. Ghil, M. R. Allen, M. D. Dettinger, K. Ide, D. Kondrashov, M. E. Mann, A. W. Robertson, A. Saunders, Y. Tian, F. Varadi, P. Yiou, Advanced spectral methods for climatic time series. *Rev. Geophys.* **40**, 3 (2002). doi:10.1029/2000RG000092
40. Cape Roberts Science Team, Studies from the Cape Roberts Project, Ross Sea, Antarctica. Scientific report of CRP-3. *Terra Antarctica* **8**, 1–308 (2001).
41. M. R. Allen, L. A. Smith, Monte Carlo SSA: Detecting irregular oscillations in the presence of colored noise. *J. Clim.* **9**, 3373–3404 (1996). doi:10.1175/1520-0442(1996)009<3373:MCSDIO>2.0.CO;2
42. F. Florindo, G. S. Wilson, A. P. Roberts, L. Sagnotti, K. L. Verosub, Magnetostratigraphy of Late Eocene-Early Oligocene strata from the CRP-3 core, Victoria Land Basin, Antarctica. *Terra Antarctica* **8**, 599–613 (2001).
43. G. Spada, P. Stocchi, SELEN: A Fortran 90 program for solving the "sea-level equation". *Comput. Geosci.* **33**, 538–562 (2007). doi:10.1016/j.cageo.2006.08.006
44. M. Rugenstein, P. Stocchi, A. von der Heydt, H. Dijkstra, H. Brinkhuis, Emplacement of Antarctic ice sheet mass affects circumpolar ocean flow. *Global Planet. Change* **118**, 16–24 (2014). doi:10.1016/j.gloplacha.2014.03.011
45. P. Stocchi, C. Escutia, A. J. P. Houben, B. L. A. Vermeersen, P. K. Bijl, H. Brinkhuis, R. M. DeConto, S. Galeotti, S. Passchier, D. Pollard, H. Brinkhuis, C. Escutia, A. Klaus, A. Fehr, T. Williams, J. A. P. Bendle, P. K. Bijl, S. M. Bohaty, S. A. Carr, R. B. Dunbar, J. A. Flores, J. J. Gonzàlez, T. G. Hayden, M. Iwai, F. J. Jimenez-Espejo, K. Katsuki, G. S. Kong, R. M. McKay, M. Nakai, M. P. Olney, S. Passchier, S. F. Pekar, J. Pross, C. Riesselman, U. Röhl, T. Sakai, P. K. Shrivastava, C. E. Stickley, S. Sugisaki, L. Tauxe, S. Tuo, T. van de Flierdt, K. Welsh, M. Yamane, Relative sea-level rise around East Antarctica during Oligocene glaciation. *Nat. Geosci.* **6**, 380–384 (2013). doi:10.1038/ngeo1783
46. K. G. Miller, J. D. Wright, R. G. Fairbanks, Unlocking the ice house: Oligocene-Miocene oxygen isotopes, eustasy, and margin erosion. *J. Geophys. Res.* **96**, 6829 (1991). doi:10.1029/90JB02015
47. S. F. Pekar, N. Christie-Blick, M. A. Kominz, K. G. Miller, Calibration between eustatic estimates from backstripping and oxygen isotopic records for the Oligocene. *Geology* **30**, 903 (2002). doi:10.1130/0091-7613(2002)030<0903:CBEEFB>2.0.CO;2
48. S. Pekar, K. G. Miller, New Jersey Oligocene "Icehouse" sequences (ODP Leg 150X) correlated with global $\delta^{18}O$ and Exxon eustatic records. *Geology* **24**, 567 (1996). doi:10.1130/0091-7613(1996)024<0567:NJOISO>2.3.CO;2
49. D. S. Wilson, S. S. R. Jamieson, P. J. Barrett, G. Leitchenkov, K. Gohl, R. D. Larter, Antarctic topography at the Eocene-Oligocene boundary. *Palaeogeogr. Palaeoclimatol. Palaeoecol.* **335–336**, 24–34 (2012). doi:10.1016/j.palaeo.2011.05.028

ACKNOWLEDGMENTS

This research is an outcome of a two-year project (PNRA 2004/4.09) partly funded by the Italian PNRA. Additional support was provided by the NSF under awards ANT-0424589, 1043018, and OCE-1202632), and NZ Ministry of Business Innovation and Employment contract C05X1001(TN). Data are available from www.pangaea.de/.

SUPPLEMENTARY MATERIALS

www.sciencemag.org/cgi/content/full/science.aab0669/DC1
Materials and Methods
Figs. S1 to S17
References (*31–49*)

9 March 2015; accepted 24 February 2016
Published online 10 March 2016
10.1126/science.aab0669

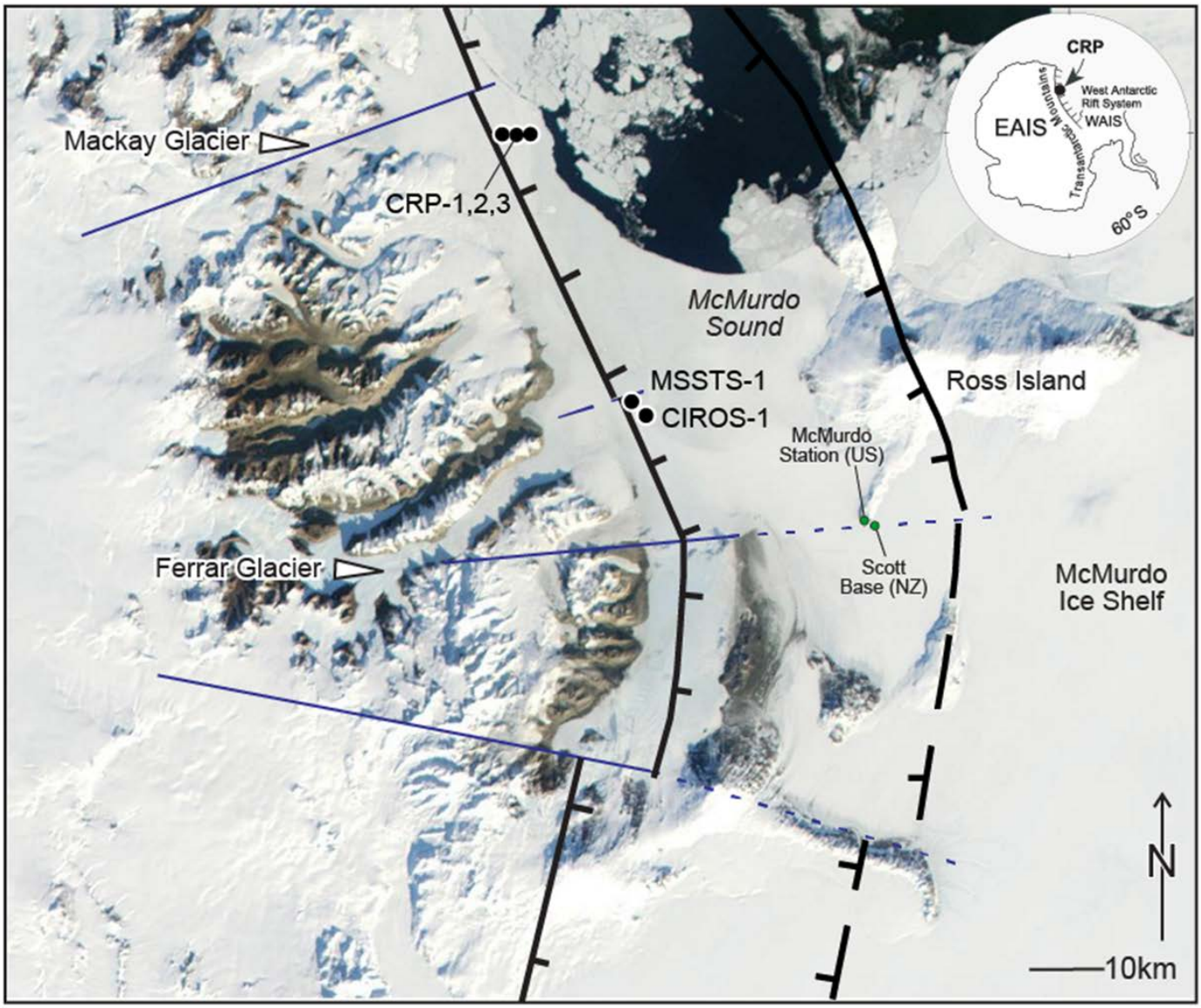

Fig. 1. Location of key geographical, geological and features in Southern McMurdo Sound. Boundary faults of the southern extension of Terror Rift are shown, together with the location of the CRP, MSSTS-1 and CIROS-1 drill sites.

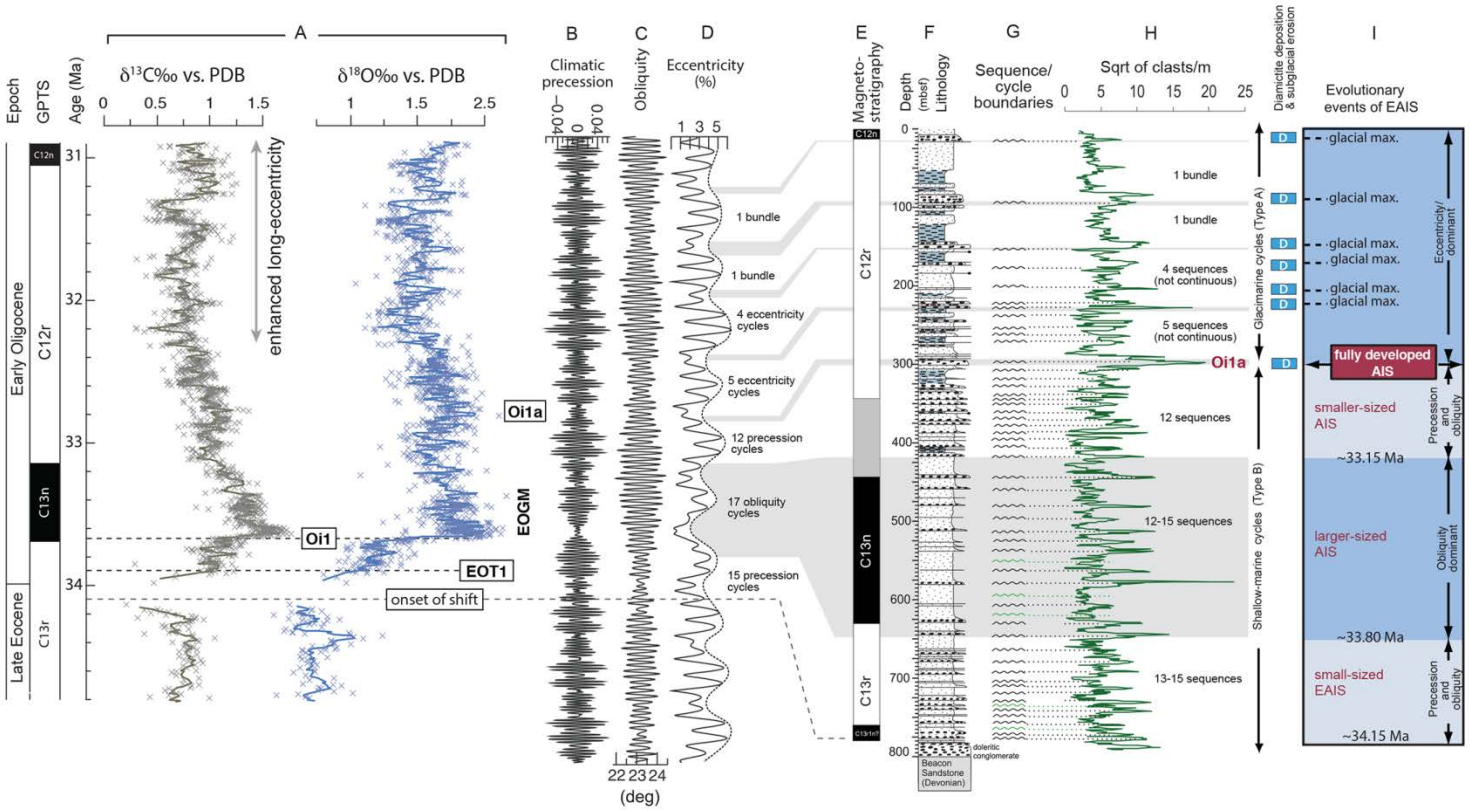

Fig. 2. Astrochronological calibration of glacial events across the Eocene-Oligocene climate transitions. (**A**) Deep-sea oxygen and carbon isotopic record from ODP Site 1218 (*2*, *17*), and time series for (**B**) climatic precession, (**C**) obliquity and (**D**) eccentricity correlated with the (**E**) magnetostratigraphy, (**F**) lithostratigraphy and (**G**) sequence stratigraphy (*13*, *15*), and (**H**) square root of clast abundance (*30*) for the Late Eocene-Early Oligocene CRP-3 drill core. Thirty-seven shallow-marine sedimentary cycles (sequences; Type B) occur in the lower 500 m of the core record, controlled by advances and retreats of land-terminating glaciers associated with <20 m sea-level oscillations. Eleven overlying glaciomarine sedimentary cycles (sequences; Type A), each bounded by glacial surfaces of erosion, occur in the upper 300 m of the CRP-3 core, and record oscillations in the extent of a more expansive marine-terminating ice sheet in Ross Embayment. (**I**) Inferred stages and events in the development of the AIS across the E-O boundary and the relationship to orbital forcing are summarized.

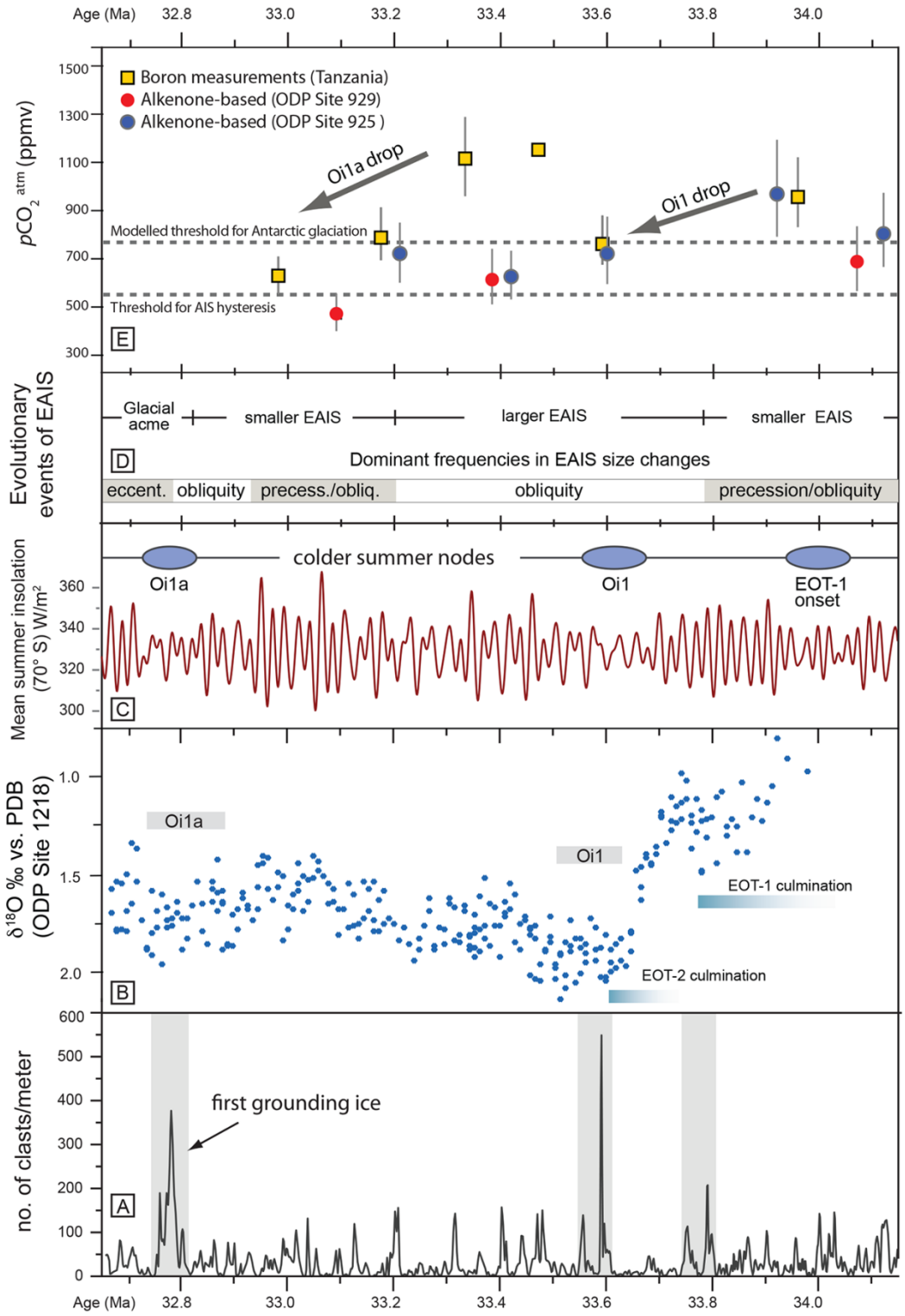

Fig. 3. Major glacial events recorded by clast abundance peaks from the CRP-3 core. (**A** and **B**) Events [grey bands in (A)] are calibrated to the astrochronologically-tuned $\delta^{18}O$ record from ODP Site1218 (B) (*2*). (**C**) Major peaks in clast abundance from CRP-3 correspond to the onset of the EOT-1 shift, and glacial maxima at the Oi1 and Oi1a, and are associated with prolonged intervals characterized by cold southern high latitude summers as expressed in the 70°S mean summer insolation. (**D**) AIS volume changes recorded by the sedimentary sequences and clast abundance (see Fig. 2) are paced by the influence of obliquity and precession on a smaller-sized terrestrial ice-sheet between 34.2-32.8 Ma. (**E**) Comparison with available atmospheric pCO_2 records based on Boron-isotope (*21*) and Alkenone (*7*) proxies shows that the first evidence of ice sheet grounding in the CRP-3 core and a major peak in clast abundance occurs at the Oi1a event (32.9-32.8 Ma), and coincides with a longer-term drop in atmospheric CO_2 drop to below ~600 ppm.